References

[1] Hoenig, S. A., "Acceleration of Dust Particles by Shock Waves," *Journal of Applied Physics*, Vol. 28, 1957, pp. 1218–1219.

[2] Carrier, G. F., "Shock Waves in a Dusty Gas," *Journal of Fluid Mechanics*, Vol. 4, 1958, pp. 376–382.

[3] Rudinger, G., "Some Properties of Shock Relaxation in Gas Flows Carrying Small Particles," *The Physics of Fluids*, Vol. 7, 1964, pp. 658–663.

[4] Kriebel, A. R., "Analysis of Normal Shock Waves in a Particle Laden Gas," *Transactions of the American Society of Mechanical Engineers, Series D: Journal of Basic Engineering*, Vol. 86, 1964, pp. 655–665.

[5] Lu, H. Y. and Chiu, H. H., "Dynamics of Gases Containing Evaporable Liquid Droplets under a Normal Shock," *AIAA Journal*, Vol. 4, No. 6, June 1966, pp. 1008–1011.

[6] Panton, R. L., "Flow Properties for the Continuum Viewpoint of a Nonequilibrium Gas-Particle Mixture," *Journal of Fluid Mechanics*, Vol. 31, 1968, pp. 273–303.

[7] Kliegel, R. B., "Gas Particle Nozzle Flows," *Ninth Symposium (International) on Combustion*, Academic Press, New York, 1963, pp. 811–826.

[8] Rudinger, G., "Experiments on Shock Relaxation in Particle Suspensions in a Gas and Preliminary Determination of Particle Drag Coefficients," *Proceedings of the Symposium on Multiphase Flow*, American Society of Mechanical Engineers, 1963, pp. 55–61.

[9] Bird, R. B., Stewart, W. E., and Lightfoot, E. N., *Transport Phenomena*, Wiley, New York, 1960.

[10] Panton, R. L. and Oppenheim, A. K., "Study of Nonequilibrium Two-Phase Flow of a Gas-Particle Mixture," Rept. AS-66-5, College of Engineering, University of Calif., Berkeley, Calif.

NOVEMBER 1968 AIAA JOURNAL VOL. 6, NO. 11

Experimental Investigation of Laminar Near Wakes behind 20° Wedges at $M_\infty = 6$

RICHARD G. BATT* AND TOSHI KUBOTA†

California Institute of Technology, Pasadena, Calif.

An experimental investigation at $M_\infty = 6$ has been conducted to determine mean-flow properties in near wakes behind several 20° included-angle wedges at zero angle of attack. One cold-wall ($H = 0.3$ in., $T_W/T_0 = 0.19$) and two adiabatic-wall ($H = 0.15$ in., $H = 0.3$ in.) configurations were tested. Freestream Reynolds numbers were varied from 0.5×10^5 to 2×10^5 per in. for each model. Flowfield mappings and flow-property profiles were obtained in the base region for the wedge of 0.3-in. base height with and without cooling by combining Pitot-pressure data with total temperature and mass flux results from hot-wire measurements. The variation of total pressure along streamlines was initially negligible during the shear-layer turning process. Downstream boundaries of these isentropic turns corresponded to viscous-layer edges that were positioned in the outer portions of the shear layers, indicating that wake shocks originated from within viscous regions of the shear layer.

Nomenclature

h = static enthalpy
H = total base height
L = surface distance to trailing edge
M = Mach number
Nu = Nusselt number
p = pressure
p_{t_2} = Pitot pressure
Re = Reynolds number
T = temperature
u = velocity
x = axial distance from model base
y = lateral distance from wake centerline
δ = boundary-layer thickness
θ = wedge included angle
ρ = density
ψ = streamline $\left(= \int_0^y \rho u dy\right)$

Subscripts

aw = adiabatic wall
b = base
C = constant
$\mathfrak{L}$ = centerline
e = edge
N = wake neck
o = reservoir conditions
sp = rear stagnation point
t = local stagnation quantity
TE = trailing edge
W = wall
ws = wedge surface
∞ = freestream

Received January 2, 1968; also presented as Paper 68-99 at the AIAA 6th Aerospace Sciences Meeting, New York, January 22–24, 1968; revision received June 3, 1968. The work discussed in this paper was carried out under the sponsorship and with the financial support of the U.S. Army Research Office and the Advanced Research Projects Agency, Contract DA-31-124-ARO(D)-33. This research is a part of Project DEFENDER sponsored by the Advanced Research Projects Agency.

* Graduate Student, Aeronautics; presently a Member of the Technical Staff at TRW Systems. Member AIAA.

† Associate Professor of Aeronautics. Member AIAA

Introduction

THE near wake behind slender bodies has been the subject of many experimental investigations for the past several years. Both shock-tunnel facilities and continuous-flow wind tunnels have been used for these investigations. Mach numbers ranging from low-supersonic to hypersonic values and flow regimes from all-laminar through transitional to fully developed turbulent flow have been examined. The primary aim has been to determine the basic structure and important scaling parameters for the base regions of hypersonic wakes and thereby define a physically realistic model for the near wake which will be amenable to analytical study. Since many of these previous experimental investigations have been

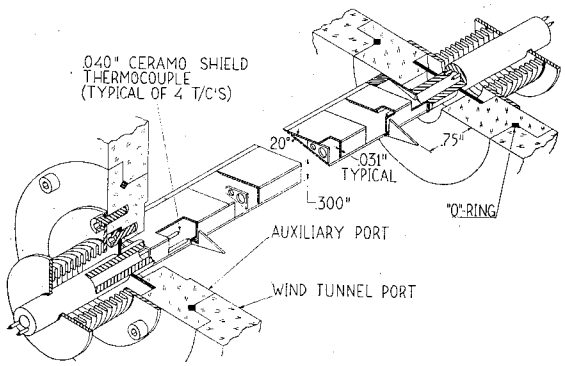

Fig. 1 20° wedge model — $H = 0.3$.

somewhat limited in the amount and type of measurements that could be obtained, it is felt that the present detailed study of the near wake (that portion of the wake upstream of and including the wake neck) with hot-wire and pitot probes and covering the effects of freestream Reynolds number, wall-temperature ratio, and model geometry will furnish an interesting supplement to the near-wake data already available.

Test Apparatus and Experimental Techniques

Wind Tunnel

Leg I of the GALCIT Hypersonic Wind Tunnel[1] with a nominal Mach number of 6 was used to obtain the set of wake measurements discussed herein. This tunnel is a continuous-flow, closed-return device with a 5-in. × 5-in. test section. A usable test rhombus extends from 23 in. (model position) to approximately 33 in. downstream of the nozzle throat. Table 1 summarizes the test conditions covered during the current experimental investigation.

Wind Tunnel Models

Three wedge models of 20° included angle have been used in the present near-wake investigation.[2] In order to isolate base-region flows from the boundary layer on the tunnel wall, triangular fences were attached to the bases of all three models. The first two models tested ($H = 0.15$ in., $H = 0.3$ in.) were fabricated from solid pieces of Ketos steel and were used primarily for base-pressure measurements. Surface-pressure data were also obtained near the trailing edge of the 0.3-in.-H model. The third model ($H = 0.3$ in.) was constructed in a rib and skin configuration in order to provide internal passage for the flow of liquid nitrogen (Fig. 1). Although this latter model was designed primarily for cold-wall testing, it was also used as an adiabatic-wall model, and a complete set of wake measurements were obtained for both cold- and adiabatic-wall conditions. The nitrogen cooling system, developed during this investigation, provided spanwise uniformity in model temperature (77°K) with only approximately 2-psig inlet pressure.[2]

Table 1 Test summary[a]

Model	p_o, psig	Re_∞/in., $\times 10^5$/in.	M_∞	T_W, °K
20° wedge	10**	0.47	6.05	350
$H = 0.15$ in.	20	0.67	5.10	
(p_b, y_N**/H only)	35**	0.94	6.11	
	50	1.22	6.11	
20° wedge $H = 0.3$ in.	60**	1.42	6.12	
	70	1.60	6.13	
(p_b, p_{ws}** only)	85**	1.90	6.14	
	100	2.18	6.15	350
20° wedge $H = 0.3$ in.	10	0.47	6.05	348
	35	0.94	6.11	350
	60	1.40	6.12	351
	85	1.90	6.14	351
20° wedge $H = 0.3$ in.	10	0.47	6.04	77
	35	0.94	6.11	77
	60	1.40	6.12	77
	85	1.90	6.14	77

[a] $T_{t_\infty} \doteq 402$°K.

Pitot-Pressure Probe

Pitot-pressure results herein were obtained with a 0.042-in.-diam probe flattened at the forward end to a 0.004-in. by 0.035-in. opening. A 5-psi Statham pressure transducer was used in most measurements to convert pressures to electrical signals that were recorded after suitable amplification on a Moseley XY recorder. Near the bases of the models, where measured pressures fell below the lower limit of the transducer's range of linearity, pitot pressures on the centerline were measured by means of a silicone-oil micromanometer.

Static-Pressure Probes

Static pressures along the wake centerline were measured with a silicone micromanometer connected to pressure probes fabricated from 0.042-in. stainless-steel tubing. The one probe with a 20° conical tip was identical to that designed and calibrated by Behrens.[3] Although this probe was used in the majority of the static-pressure measurements, its tip-to-orifice length prevented taking measurements near the base of a model, and three additional probes were used to obtain the base-region data. These probes consisted of 2-in. lengths of 0.042-in. tubing with one end capped off. On each probe, two orifices were located at a prescribed distance from the capped tip and the open end was soft-soldered to a pressure-lead holder. In practice, the sealed tip of the probe was placed in contact with the base of the model on the wake centerline and the pressure recorded by a precision micromanometer. Since tip-to-orifice lengths were different for each of the three probes, it was possible to obtain a distribution of static pressures on the wake centerline.

Hot-Wire Anemometer

The hot-wire probes used for the present set of measurements were similar to those designed by Dewey[4] and modified by Herzog.[5] Each probe consisted of platinum-10% rhodium wire (0.0001-in.-diam) approximately 0.030 in. in length, soft-soldered to two needle supports. Chromel-Alumel thermocouple wires (0.001-in.-diam) were spot welded to within 0.005 in. of the tip of one needle. All wires were annealed

Table 2 Accuracy summary

Quantity	Over-all uncertainty
Measured data	
p_{t_2}/p_0	±2%
$p_{\text{℄}}/p_\infty$	±2%
T_{aw}	±1%
Nu_t	±3%
p_b/p_∞ (base)	±4%
p_b/p_∞ (℄ probe-low Re)	+7%, −0%
p_{ws}/p_∞	±2%
$(x/H)_{sp}$	±0.1H
Derived result	
T_t/T_o (max—adiabatic wall)	±2%
T_t/T_o (max—cold wall)	±4%
$\rho u/\rho_\infty u_\infty$	±5%
p/p_∞, p_t/p_o	±20%
x,y	±0.005 in.
$\psi/\rho_\infty u_\infty H$, $(T_t/T_o)_c$, $(p_t/p_o)_c$	$0 \le x/H \le 0.25$: ±0.01H; $x/H > 0.25$: ±0.02H

and calibrated in the manner outlined by Dewey.[4] From these calibration measurements, temperature coefficients of electrical resistivity and reference resistances for zero electrical current were determined. The hot-wire data were obtained by means of an instrumentation system[4] that automatically positioned the probe in the tunnel and recorded on IBM cards the probe position, support temperature, and wire voltages corresponding to five predetermined heating currents.

Data Reduction and Accuracy Estimates

Corrections to Measured Data

All pitot- and static-pressure results herein include corrections for axial gradients in test-section pressure, virtual-leak phenomena, and viscous-interaction effects.[2] A description of the manner in which hot-wire raw data have been reduced, corrected, and finally combined with recovery-temperature and Nusselt-number calibration data to provide local stagnation temperature and mass flux data for the flow in question is presented in Ref. 2. Table 2 summarizes estimated uncertainty factors for all measured data and derived results which are of interest to the present study.

Mean-Flow Calculations

By combining corrected data with the compressible-flow relations[6] mean-flow calculations have been carried out for the current investigation. All calculations were performed on the IBM 7094 using semiprofile traces of pitot pressure and total temperature along with a third independently measured quantity. For those portions of the near wake between the wake shock waves wherein lateral gradients in static pressure were found to be negligible, this third quantity was the centerline static pressure. All other shear-layer data were computed by using semiprofile traces of mass flux in place of static pressures. In the regions of inviscid flow located between the nose shock and the shear-layer edge, total temperatures and total pressures remained constant throughout since all streamlines were assumed to have suffered the same total head loss in passing through the leading-edge shock. As a result, the mean-flow properties for these regions were computed from freestream total temperatures, measured pitot pressures, and total pressures, as calculated from the nose-shock orientation and freestream conditions. Clearly, curvature of the nose-shock wave near the model's leading edge invalidates the assumption of isentropic flow in the above inviscid regions. However, even with the resulting error in total pressure, derived mean-flow results are still within the accuracy limits of Table 2, and thus the assumption of uniform stagnation pressure was considered reasonable. Streamline calculations for the base region were performed by integrating mass flux data from the nose shock toward the wake centerline. Since near the wake centerline such a procedure results in appreciable errors, additional streamline data were obtained by integrating from the centerline out to the wake shock using the assumption of negligible lateral gradient in static pressure.

Results and Discussion

The far-wake transition results reported in Ref. 2 were obtained prior to initiating the near-wake investigation discussed in the present paper. In this transition study, it was found that base-region flows were laminar for all adiabatic-wall tests and at least for the two lowest test Reynolds numbers of the cold-wall wedge. Reference 2 also contains complete mean-flow results for both the near and far wakes behind the present wedge configurations. Because of space limitations, however, it is necessary to publish the far-wake data in the open literature at some future date and to present herein only selected samplings of the near-wake results.

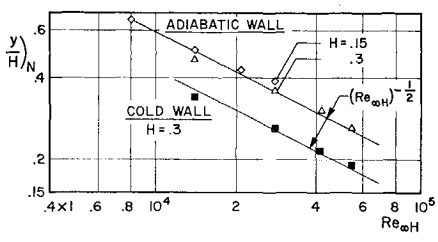

Fig. 2 Wake neck thickness.

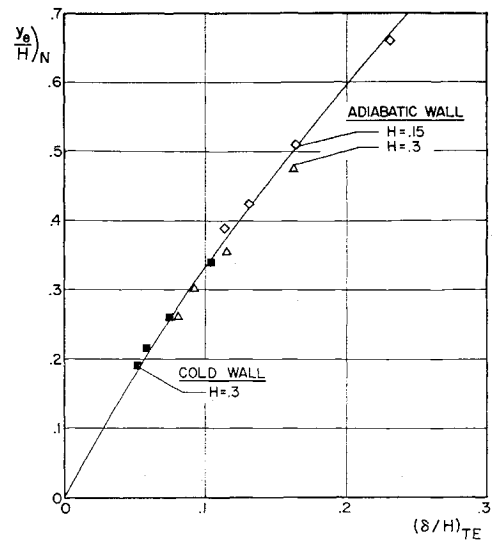

Fig. 3 Neck thickness correlation.

Neck Thickness

By examining wake growth data,[2] neck thicknesses (minimum value of wake thickness) have been determined for all three wedge configurations, and the results are presented in Fig. 2 as a function of the Reynolds number. Consistency of the adiabatic-wall results is evident in that the data for both the $H = 0.15$-in. and $H = 0.3$-in. wedges coincide in a favorable manner. Although the neck thickness data in Fig. 2 illustrate that a correlation with Reynolds number exists, it is also apparent that, when presenting the data in this manner, the adiabatic- and cold-wall data result in two separate curves. However, if the data are replotted against the thickness of the trailing-edge boundary layer, both the adiabatic- and cold-wall data collapse to one curve (Fig. 3). This result additionally verifies Chapman's finding[7] that the boundary-layer thickness at the trailing edge represents an important length scale for near-wake flows.

Wedge Surface Pressure

The upstream influence of the low base pressure on wedge surface pressures is illustrated in Fig. 4. These adiabatic-wall data indicate that the flow first "senses" low base pressures roughly two to three boundary-layer thicknesses upstream of the base. Also shown on the figure for comparison purposes are wedge pressures corresponding to the trailing-edge distance as determined using Kendall's results from his investigation of hypersonic flow over a flat plate.[8]

Wedge Base Pressure

The results of base-pressure measurements for the three wedge models are presented in Fig. 5. These data show the variation of base pressure with trailing-edge Reynolds number based on fluid properties determined from inviscid-flow theory. Also shown in the figure are the data of Dewey for both 30° and 45° adiabatic wedges.[9] A significant decrease in base pressure with increasing Reynolds number is evident from both Dewey's and the present results. Results from

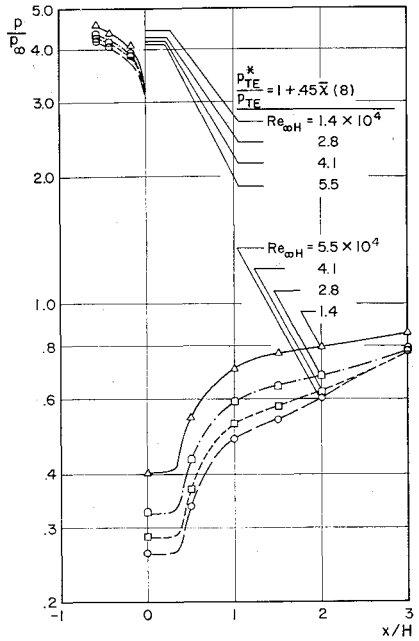

Fig. 4 Pressure distribution on wedge surface near trailing edge and along wake centerline for 20° adiabatic-wall wedge.

both the small ($H = 0.15$ in.) and large ($H = 0.3$ in.) adiabatic wedges correlate successfully on this basis.

Since Chapman[7] as well as others have pointed out the dependence of base pressure on the boundary-layer thickness at the trailing edge, and, further, because a successful correlation of neck thickness for both adiabatic- and cold-wall results has been achieved with this scaling parameter, a correlation of the base-pressure data has also been made with this length scale, and the results are shown in Fig. 6. For the adiabatic-wall data the weak-interaction theory modified in accordance with Kendall's results has been used to determine $(\delta/H)_{TE}$. On the other hand, the boundary-layer thickness at the trailing edge of the cold-wall wedge is based on Chapman-Rubesin boundary-layer theory for arbitrary wall temperature.[10] Base-pressure estimates[2] determined from the Chapman theory have been made for $\theta = 45°$ and $\theta = 20°$ and for both zero (Chapman[11]) and finite (Denison and Baum[12]) initial boundary-layer thickness. Although the Chapman estimates on Fig. 6 show no variation with Reynolds numbers, the over-all levels seem to compare favorably with the measured data for an "efficiency factor" of one.[2]

The method of correlation used in Fig. 6 still retains the wedge angle as an explicit variable in the base-pressure determination. However, as was found in correlating the neck thickness data discussed previously, the important fact indicated by the results shown in Fig. 6 is the collapsing of both the adiabatic-wall and cold-wall base-pressure data from the present investigation to a single curve. This result further

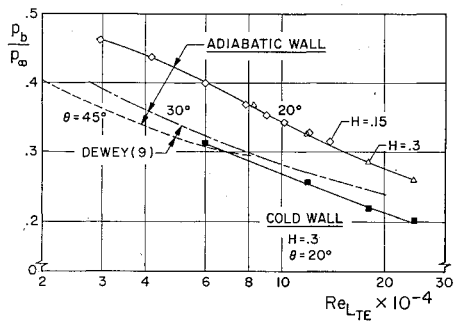

Fig. 5 Wedge base pressure.

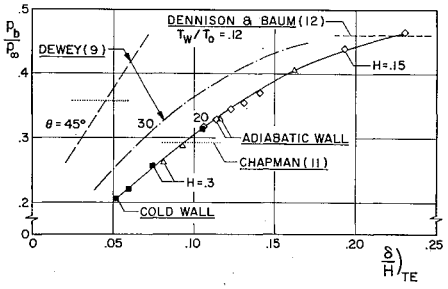

Fig. 6 Correlation of wedge base pressure data.

substantiates the significance of the boundary-layer thickness at the trailing edge as a suitable length scale for the base-flow problem.

In an effort to determine additional characteristic parameters for the base pressure, several other combinations of variables have been attempted. One finding is that all adiabatic-wall data from both Dewey's and the present studies collapse to one curve with only ±7% scatter by plotting p_b/p_∞ as a function of the freestream Reynolds number based on the base height (Fig. 7). This result, indicating only minor dependence on wedge angle, was similarly found by Cheng et al.[13] in their experimental investigation of wakes behind wedges in low-density flow.

Rear Stagnation Point

The rear stagnation point is the point on the wake axis where the flow stagnates and separates the reverse flow in the base region from the downstream wake. For the present results, the rear stagnation point was determined by plotting static and pitot pressures along the wake centerline as a function of axial distance (Fig. 8). In the present set of measurements, with the wedge of 0.3 in base height, the rear stagnation point was located at $x/H = 0.75 \pm 0.1$ for both adiabatic- and cold-wall conditions.[2] This result was confirmed, for the adiabatic-wall configuration, by use of the differential-pressure probe discussed in Ref. 2. Both of these methods for determining the rear stagnation point have been used by Martellucci et al.[14] in their experiments on the turbulent near wake of a cone at $M_\infty = 6$, and similar agreement between the two techniques was obtained. The present results, $x/H = 0.75$, are in good agreement with the summary curve of Ref. 14 showing the variation of the location of rear stagnation point with the trailing-edge Reynolds number. Similarly, for the cold-wall configuration, the temperature at the rear stagnation point ($T_{sp}/T_o = 0.34$) compares favorably with previous cold-wall data.[2]

Shear-Layer Profiles

Typical shear-layer profiles, all from the low-Reynolds-number adiabatic-wall case, are plotted in Fig. 9 in overlap fashion with the base geometry, so as to illustrate the manner in which characteristic lines and/or regions are distinguishable. For example, the upper half of Fig. 9 presents total temperature profiles for the near-wake shear layer, and the

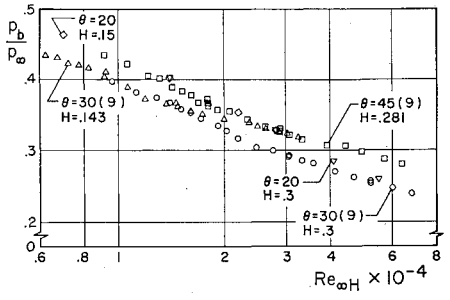

Fig. 7 Base pressure correlation for adiabatic-wall wedge.

location where the total temperature becomes equal to the freestream total temperature represents the shear-layer edge. The one open symbol shown in Fig. 9 on the model surface at $x/H = -0.5$ corresponds to a calculated boundary-layer thickness based on the theory of Ref. 10. This thickness agrees favorably with similar thickness estimates based on the weak-interaction theory. An interesting result of these total temperature data is the location and variation of the shear-layer's edge with axial distance. Not only is the wake neck [$5 \leq (x/H)_N \leq 7$, Ref. 2], defined as the wake's minimum thickness location, not located near the wake's rear stagnation point, but it occurs even downstream of the centerline sonic point.

The bow-shock and wave-shock positions indicated in Fig. 9 were determined from transverse pitot-pressure traces. For all cases, the lip shock formed during the base separation process coalesced with the wake shock to form a single shock structure. The $u = 0$ line of Fig. 9 corresponds to those transverse locations where the static pressure, as measured on the wake's centerline, and pitot pressure are equal.

All the static-pressure data in the lower half of Fig. 9, represented by open symbols and below the shear-layer edge, were arrived at by combining pitot pressures with total temperatures and mass flux data from hot-wire measurements. Within the accuracy limits specified in Table 2, the results indicate that the static pressure is constant from the centerline out to the wave shock and also that the static pressure, at least for $x/H = 1.5$, from the wake shock out to the shear-layer edge is constant and equal to the base pressure. The data near the corner show that the effects of the corner expansion become progressively more dominant within the shear layer, until at the trailing edge, the entire shear layer from the edge down to the zero-velocity line is experiencing large lateral-pressure gradients. Thus, the shear layer cannot be considered as a region of constant transverse pressure until several boundary-layer thicknesses downstream of the base. Figure 9 also shows the approximate locations of the leading and trailing rays of the corner expansion fan defined by the methods of tangents indicated on the figure. The leading ray orientation determined in this manner agrees with the Mach wave angle for the wedge flow of the present investigation. In the shear layer, a slight curvature of this line is observed. The Mach wave angles for the local flow along the trailing ray have been compared with the orientation of the trailing ray itself and a satisfactory agreement was obtained. The extent of upstream influence determined by extrapolating the leading

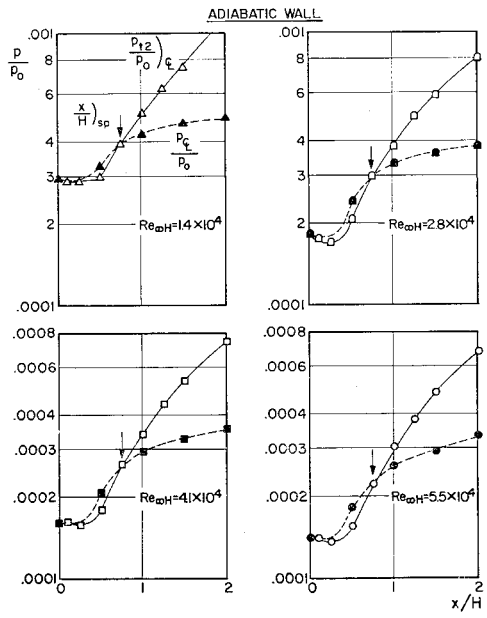

Fig. 8 Rear stagnation-point location.

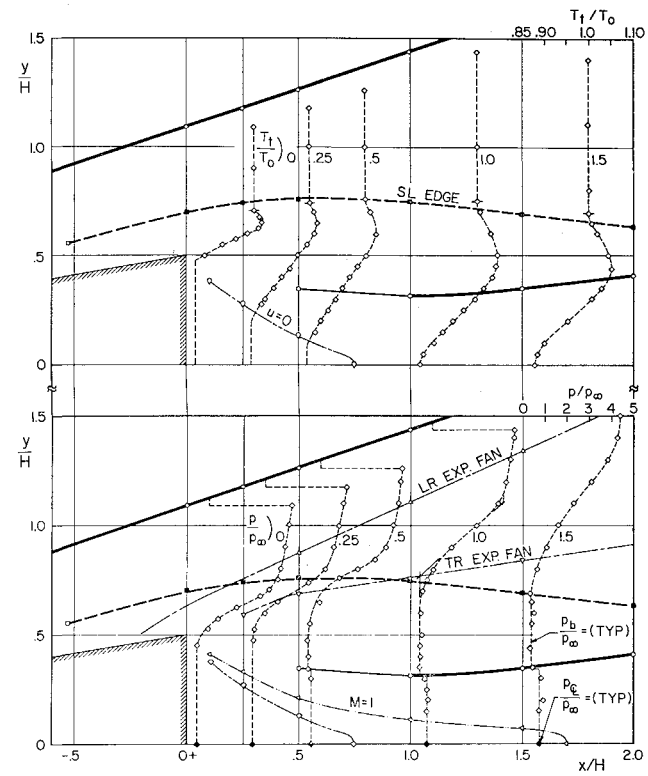

Fig. 9 Typical shear-layer profiles for near wake behind 20° adiabatic-wall wedge at $Re_{\infty H} = 1.4 \times 10^4$.

ray of the expansion fan agrees in general with the results of the surface pressure measurements discussed earlier. The sonic line shown in Fig. 9 is the locus of the points where the ratio of centerline static pressure to pitot pressure corresponds to the value at Mach number unity. For all cases investigated herein, the centerline sonic point was located between one and a half and two base heights downstream of the model base.

Near-Wake Flowfield Mappings

Several flowfield mappings from the present near-wake investigations are shown in Figs. 10 and 11. These figures not only indicate the location of the characteristic lines discussed in the previous section, but also illustrate the relative orientation of streamlines, constant-total-pressure lines and, as in the case of the cold-wall wedge, lines of constant-total temperature. Additional calculations of flow direction relative to the shock wave were made by combining pitot pressures, both upstream and downstream of the wake shock, with centerline pressure data. The resulting orientation angles of the flow are indicated by the short lines drawn to the shock location symbols. The comparison between the streamlines and these flow direction lines is seen to be very favorable.

The tendency of the flow not to turn sharply at the base is clearly shown in all the figures. The mass flow within the lower portions of the shear layer is thus very small. The resulting low Reynolds numbers then suggest that any viscous layer that is developing within the shear layer will experience an appreciable growth rate. Using the locus of points where the total-pressure lines begin to diverge from the streamlines as a rough estimate for the location of the outer edge of this viscous layer, it is seen that a large growth rate does indeed occur. The fact that within the shear layer the total pressures remain almost invariant along streamlines for some distance downstream of the corner confirms the isentropic turn postulated in some analytical studies. At one time it had been speculated that the viscous layer was contained within the wake-shock boundaries and that inviscid-rotational characteristic methods could then be utilized for the flow be-

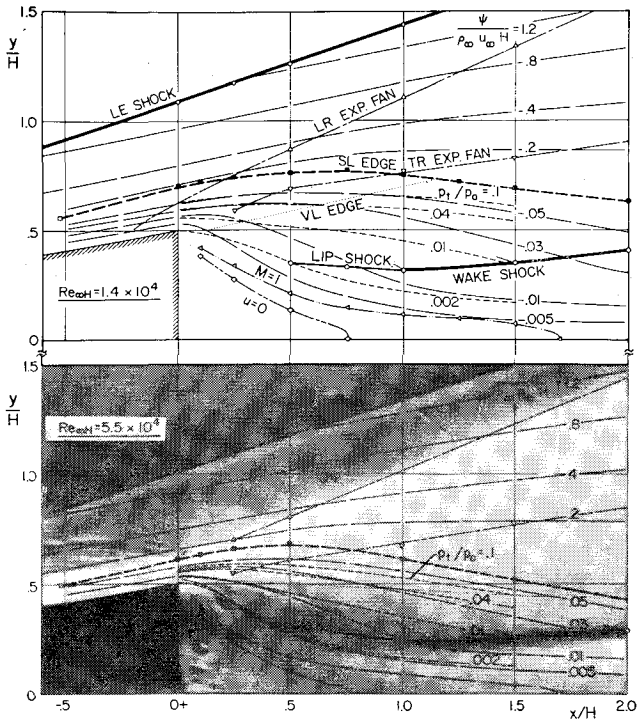

Fig. 10 Flowfield mapping of near wake behind 20° adiabatic-wall wedge.

tween the wake shock and shear-layer edge. It is seen that this analytical model is open to question since the wake shock now appears to be imbedded within the viscous layer itself. Although the viscous-layer edge moves toward the wake shock with increasing Reynolds number and cooling, it was distinctly above the wake shock even at the highest Reynolds number for the cold-wall case.[2] The total-temperature lines exhibited in Fig. 11 indicate only minor variations of total temperature along streamlines outside the base-region shock boundaries.

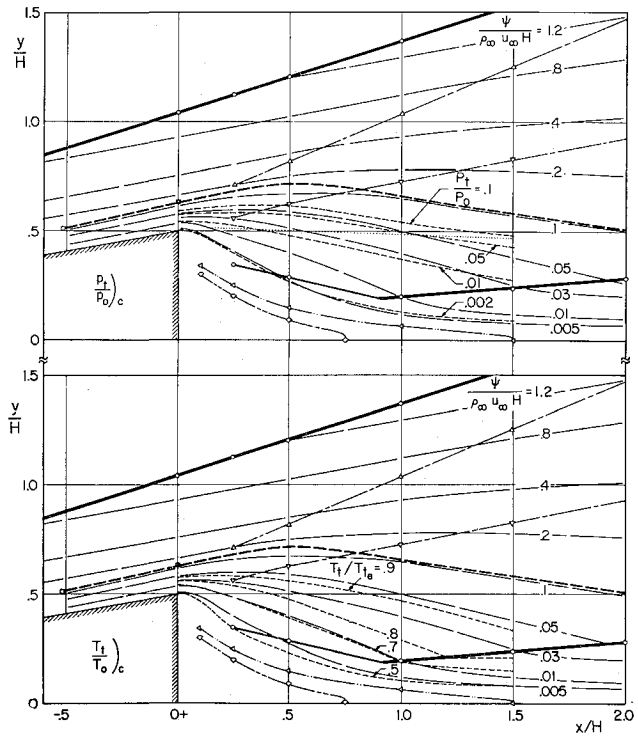

Fig. 11 Flowfield mapping of near wake behind 20° cold-wall wedge at $Re_{\infty H} = 1.4 \times 10^4$ ($T_W/T_o = 0.19$).

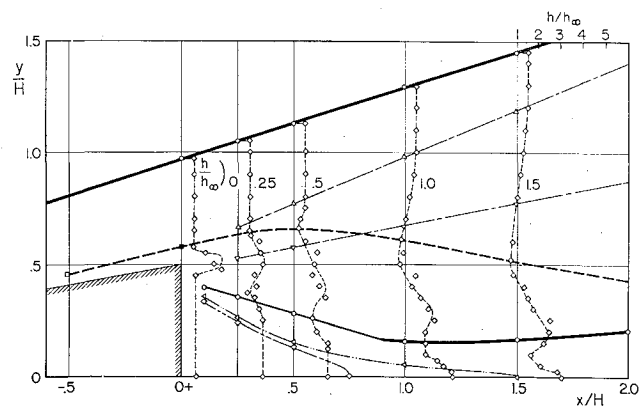

Fig. 12 Static enthalpy profiles for near wake behind 20° cold-wall wedge at $Re_{\infty H} = 5.5 \times 10^4$.

The extrapolation of the lip shock, sonic line, and zero-velocity line toward the model base indicates that flow separation appears to occur not at the base corner, but at some distance below the corner as experiments of Hama[15] have indicated. In addition, these figures show that the shear-layer edges and wake shocks move toward the centerline with increasing Reynolds number and model cooling. Also, with cooling, the point at which the lip shock first becomes discernible is located farther upstream than for the low-Reynolds-number adiabatic-wall cases. This result is evident from the complete pitot-pressure profile data.[2] With regard to the lip-shock strength, a pressure jump at $x/H = 1.0$ of 1.75 to 2 exists for all the near-wake results of Figs. 10 and 11. These values are in good agreement with Hama's correlation of wedge data[15] and further substantiate his claim that lip shocks found in near wakes behind slender bodies are not necessarily weak.

In the lower half of Fig. 10, the mapping for the high-Reynolds-number adiabatic-wall case has been superimposed on a schlieren photograph of the near wake behind a 20° wedge under virtually the same free-stream conditions. The locations of the nose and wake shocks and the leading ray of the expansion fan, as determined by the flowfield mapping and those as shown by the schlieren photograph, are seen to be in very favorable agreement. A similar comparison regarding the wedge boundary layer was not possible because light reflections due to slight model misalignment obscured the boundary layer along the wedge surface in the schlieren photograph. The large density gradients in the expansion fan and in the shear layer itself are clearly shown by the "white shading" of the schlieren portion of Fig. 10. This figure illustrates the difficulty of locating shear-layer edges in schlieren photographs for these high-speed wake flows. At lower supersonic speeds and even for hypersonic flows behind blunt bodies where density gradients immediately outside the shear-layer edge become negligibly small, the edge of the shear layer is easily discernible. For these latter flows, the corner expansion fan does not extend into the separated shear layer in the manner shown by the present flowfield mappings. For slender bodies with flat bases, this result represents a major distinction between supersonic and hypersonic near-wake flows.

Static Enthalpy Profiles in Near Wake of Cold-Wall Wedge

Figure 12 shows static-enthalpy distributions at the highest Reynolds number investigated for the cold-wall wedge. In boundary layers on a cold wall, a local temperature peak, or "hot spot," exists within the boundary layer. The existence of similar off-axis hot spots has been postulated also in near wakes behind cold bodies. Not only is the off-axis peak evident in Fig. 12 but its initial magnitude ($h/h_\infty \doteq 2.8$)

compares quite favorably with the maximum value calculated by the theory of Ref. 10 for a laminar boundary layer with heat transfer. In addition, it appears that the location of this peak at each axial station indicates that such hot spots follow along streamlines. Additional static-enthalpy data[2] further illustrate that the noted hot spots coalesce with centerline temperature peaks within two base heights downstream from the model base.

Summary of Results

An experimental investigation at $M_\infty = 6$ has been conducted to determine mean-flow properties in laminar near wakes behind 20° included-angle wedges at zero angle of attack with and without cooling. The Reynolds number based on the freestream condition and the base height were varied from 0.75×10^4 to 6×10^4. The main results which were obtained from this investigation are as follows:

1) A collapsing of adiabatic- and cold-wall results into one curve was accomplished for both the wake neck thickness and base-pressure measurements by plotting these data as functions of the trailing-edge boundary-layer thickness. A trend of increasing base pressure with increase in boundary-layer thickness was observed. These results reemphasized that the boundary-layer thickness at the trailing edge represents an important length scale for the near-wake problem.

2) Rear stagnation points and centerline sonic points were located approximately three-quarters and one-and-three-quarters base heights, respectively, downstream of the model base for all cases. The temperature at the rear stagnation point for the cooled wedge ($T_W/T_o = 0.19$) was 0.34 of the freestream stagnation temperature for all Reynolds numbers.

3) For the cooled wedge, peaks in static temperatures occurred in the shear layers outside the wake-shock structure. Initial magnitudes of these peak temperatures agreed favorably with estimates from laminar boundary-layer theory. These hot spots followed along streamlines and coalesced with centerline temperature peaks within two base heights downstream from the model base.

4) Wake shocks, shear-layer edges, base-region sonic lines, and viscous-layer edges moved closer to the wake centerline with increasing Reynolds number and decreasing wall temperature.

5) The boundary layer on the wedge surface was influenced by the low base pressure two to three boundary-layer thicknesses upstream of the base. The lip shock formed during the boundary-layer separation process coalesced with the wake recompression shock to form a single shock structure.

6) Most of the outer flow of the separated boundary layer turned very slowly in the vicinity of the base, such that the amount of mass flow contained within the base region proper corresponded to a small fraction (5%) of the total boundary-layer flow. This turning of the separated boundary layer, although gradual, caused appreciable lateral-pressure gradients in the shear layers in the vicinity of the corner. These gradients became negligible once the flow had progressed several boundary-layer thicknesses downstream of the base. Downstream of this region of nonzero pressure gradient and above the wake shock, static pressures were constant and equivalent to the base pressures.

7) Inside the wake shocks, lateral-pressure gradients were negligible.

8) Initially, during the corner turning process, the variation of total pressure along streamlines was negligible. The downstream boundaries of these isentropic turns corresponded to viscous-layer edges that were positioned in the outer portions of the shear layers indicating that wake shocks originated from within viscous regions of the shear layers.

References

[1] Baloga, P. E. and Nagamatsu, H. T., "Instrumentation of GALCIT Hypersonic Wind Tunnels," Memo. 29, July 31, 1955, Graduate Aeronautical Lab., California Institute of Technology, Pasadena, Calif.

[2] Batt, R. G., "Experimental Investigation of Wakes Behind Two-Dimensional Slender Bodies at Mach Number Six," Ph.D. thesis, 1967, California Institute of Technology, Pasadena, Calif.

[3] Behrens, W., "Viscous Interaction Effects on a Static Pressure Probe at $M = 6$," *AIAA Journal*, Vol. 1, No. 12, Dec. 1963, pp. 2364–2366.

[4] Dewey, C. F., Jr., "Hot Wire Measurements in Low Reynolds Number Hypersonic Flows," *ARS Journal*, Vol. 31, No. 12, Dec. 1961, pp. 1709–1718; also Dewey, C. F., Jr., "A Correlation of Convective Heat Transfer and Recovery Temperature Data for Cylinders in Compressible Flow," *International Journal of Heat and Mass Transfer*, Vol. 8, 1965, pp. 245–252.

[5] Herzog, R. R., "Nitrogen Injection into the Base Region of a Hypersonic Body," Hypersonic Research Project Memo. 71, Aug. 1964, Graduate Aeronautical Lab., California Institute of Technology, Pasadena, Calif.

[6] Ames Research Staff, "Equations, Tables and Charts for Compressible Flow," Rept. 1135, 1953, NACA.

[7] Chapman, D. R., "An Analysis of Base Pressure at Supersonic Velocities and Comparison with Experiment," Rept. 1051, May 1950, NACA.

[8] Kendall, J. M., Jr., "An Experimental Investigation of Leading-Edge Shock-Wave Boundary Layer Interaction at M = 5.8," *Journal of the Aerospace Sciences*, Vol. 29, No. 8, Aug. 1966, pp. 961–968.

[9] Dewey, C. F., Jr., "Near Wake of a Blunt Body at Hypersonic Speeds," *AIAA Journal*, Vol. 3, No. 6, June 1965, pp. 1001–1010.

[10] Chapman, D. R. and Rubesin, M. W., "Temperature and Velocity Profiles in the Compressible Laminar Boundary Layer with Arbitrary Distribution of Surface Temperature," *Journal of the Aeronautical Sciences*, Vol. 16, No. 9, Sept. 1949, pp. 547–565.

[11] Chapman, D. R., Kuehn, D. M., and Larson, H. F., "Investigation of Separated Flows in Supersonic and Subsonic Streams with Emphasis on the Effect of Transition," Rept. 1356, 1958, NACA.

[12] Dennison, M. R. and Baum, E., "Compressible Free Shear Layer with Finite Initial Thickness," Paper 62-125, June 1962, IAS.

[13] Cheng, R., Schaaf, S. A., and Hurlbut, F. C., "The Measurement of Base Pressure of Wedges in Supersonic Low Density Flow," Rept. AS-64 17, Nov. 1964, Institute of Engineering Research, University of California, Berkeley.

[14] Martellucci, A., Trucco, H., and Agnone, A., "Measurements of the Turbulent Near Wake of a Cone at Mach 6," *AIAA Journal*, Vol. 4, No. 3, March 1966, pp. 385–391.

[15] Hama, F. R., "Experimental Investigations of Wedge Base Pressure and Lip Shock," TR 32-1033, Dec. 1966, Jet Propulsion Lab., Pasadena, Calif.